



**Distance-Dependent Fluorescence of
Tris(bipyridine)ruthenium(II) on Supported Plasmonic Gold
Nanoparticle Ensembles**

Journal:	<i>Nanoscale</i>
Manuscript ID:	NR-ART-07-2014-004237.R1
Article Type:	Paper
Date Submitted by the Author:	15-Oct-2014
Complete List of Authors:	Kedem, Ofer; Weizmann Institute of Science, Dept. of Materials and Interfaces Wohlleben, Wendel; BASF SE, Dept. of Material Physics Rubinstein, I; Weizmann Institute of Science, Dept. of Materials and Interfaces

ARTICLE

Distance-Dependent Fluorescence of Tris(bipyridine)ruthenium(II) on Supported Plasmonic Gold Nanoparticle Ensembles

Cite this: DOI: 10.1039/x0xx00000x

Ofer Kedem,^{*a} Wendel Wohlleben^b and Israel Rubinstein^aReceived 00th January 2014,
Accepted 00th January 2014

DOI: 10.1039/x0xx00000x

www.rsc.org/

Metal surfaces and nanostructures interact with fluorescent materials, enhancing or quenching the fluorescence intensity, modifying the fluorescent lifetime, and changing the emission frequency and linewidth. These interactions occur via several mechanisms, including radiationless energy transfer, electric field enhancement, and photonic mode density modification. The interactions display a strong dependence on the distance between the fluorophore and the metal structures. Here we study the distance-dependent effects of two types of plasmonic gold nano-island films on the emission intensity, wavelength, linewidth and lifetime of a fluorophore layer, separated from the film by a dielectric spacer 2–348 nm thick. The distance dependence is found to be unrelated to the plasmonic field decay lengths. In some cases fluorescence intensity enhancement is seen even at 200 nm metal-fluorophore separation, indicating far-field effects. We report, for the first time, a distance-dependent oscillation in the emission peak wavelength and linewidth, attributed to interference-based oscillations in the intensity of the electric field. We find that the studied nanoparticle (NP) films do not display the previously reported distance profile of single NPs, but rather behave in a collective fashion similar to continuous metal surfaces.

1. Introduction

The interaction between plasmonic nanostructures, *e.g.*, metal nanoparticles (NPs), and fluorescent species, has been the subject of considerable research.^{1–4} Proximity of such nanostructures to fluorophores such as organic dyes, metal complexes, or quantum dots can cause either quenching or enhancement of the fluorescence, a phenomenon frequently referred to as *metal-enhanced fluorescence* (MEF). The type and magnitude of the effect are dependent on multiple parameters, including the distance between the nanostructures and the fluorophores,^{5–7} the composition of the metal,⁸ the size and shape of the NPs,^{9,10} the properties of the fluorophore itself (*e.g.*, quantum yield), the overlap of the fluorophore absorption and emission bands with the plasmon band,^{11,12} and even the type of adhesion layer used for the metallic nanostructures.¹³ Metal nanostructures have also been found to decrease self-quenching in nearby fluorophores,^{14–16} and in some cases can significantly alter the shape of their emission spectrum.¹⁷ MEF is widely studied for bio-sensing applications, where it can result in better sensitivity and lower detection limits.¹⁸ The sensitivity of MEF to the fluorophore-nanostructure separation can provide the basis for ruler systems, as in recent work by Bourret *et al.*, who studied the modification of the fluorescence

spectral shape by a nearby plasmonic particle.¹⁹ Anger *et al.* demonstrated the distance-dependent transition from enhancement at longer ranges to quenching at very short separations, for a single-molecule/single-NP system.²⁰

The quantum efficiency and lifetime of a fluorophore are determined by its rates of decay to the ground state,³

$$\eta = \frac{\Gamma_r}{\Gamma_r + \Gamma_{nr}^0 + \Gamma_{ET}} \quad (1)$$

where η is the quantum efficiency, Γ_r is the radiative decay rate, Γ_{nr}^0 is the intrinsic non-radiative decay rate, and Γ_{ET} is the rate of (radiationless) energy transfer to the metal. The observed lifetime is given by:

$$\tau = \frac{1}{\Gamma_r + \Gamma_{nr}^0 + \Gamma_{ET}} \quad (2)$$

The transition rate is governed by Fermi's golden rule,^{21,22}

$$\Gamma_{ij} \propto |M_{ij}|^2 \rho(\nu_{ij}) \quad (3)$$

where Γ_{ij} is the transition rate between states i and j , M_{ij} is the matrix element connecting the states (determined by their associated wavefunctions), and $\rho(\nu_{ij})$ is the density of states at the transition frequency. As a result, modulating the density of states modifies the transition rate, and ultimately the fluorescence quantum yield.

The total fluorescence yield $F(\lambda_{\text{ex}}, \lambda_{\text{em}})$ also depends on the excitation process. The latter can be modified in the vicinity of plasmonic NPs, due to increased electric field strength,

$$F(\lambda_{\text{ex}}, \lambda_{\text{em}}) = \frac{\lambda_{\text{ex}} I(\lambda_{\text{ex}})}{hc} \sigma_{\text{abs}}^{\text{eff}}(\lambda_{\text{ex}}) \eta(\lambda_{\text{em}}) \quad (4)$$

where λ_{ex} and λ_{em} are the excitation and emission wavelengths, $I(\lambda_{\text{ex}})$ is the intensity of the excitation beam, and $\sigma_{\text{abs}}^{\text{eff}}(\lambda_{\text{ex}})$ is the effective absorption cross-section,

$$\sigma_{\text{abs}}^{\text{eff}}(\lambda_{\text{ex}}) = \frac{|\vec{p} \cdot \vec{E}(\lambda_{\text{ex}})|^2}{|\vec{p} \cdot \vec{E}^0(\lambda_{\text{ex}})|^2} \sigma_{\text{abs}}^0(\lambda_{\text{ex}}) \quad (5)$$

where \vec{p} is the molecular dipole moment, $\vec{E}(\lambda_{\text{ex}})$ and $\vec{E}^0(\lambda_{\text{ex}})$ are the electric fields in the presence and absence of a metallic nanostructure, respectively, and $\sigma_{\text{abs}}^0(\lambda_{\text{ex}})$ is the intrinsic absorption cross-section of an unperturbed fluorophore. $\vec{E}(\lambda_{\text{ex}})$ can be increased, decreased, or reoriented with respect to $\vec{E}^0(\lambda_{\text{ex}})$.³

Fluorophore-fluorophore energy transfer is commonly interpreted as *Förster resonance energy transfer* (FRET), which predicts an R^{-6} distance dependence, and so is effectively limited to a few nm. However, NP-fluorophore interactions exhibit a longer effective distance, better described by alternative models, with an R^{-4} distance dependence.¹² Thus, non-radiative energy transfer in NP-fluorophore systems plays a greater part in quenching, over longer distances, than in molecular systems. Beside energy-transfer, charge-transfer between the metal nanoparticle and the fluorophore can result in fluorescence quenching at very short (tunnelling) distances.^{23,24}

In most published data concerning MEF with plasmonic NPs, the distance profile spans at most several tens of nanometers, with no interaction at longer distances.^{6,8,25-29} In this work, we focus on the interaction of fluorophore monolayers at a wide range of separations (2 - 348 nm) from the metal surface in metal NP films. The latter are similar in certain ways to continuous metallic films,³⁰ allowing us to exploit the considerable theoretical and experimental literature treating MEF with the latter.^{1,3,31-35} Several theoretical approaches have been used to model the interaction, including work by Drexhage *et al.*,³⁶ Chance, Prock and Silbey,³⁷ Gersten and Nitzan,³⁸ Ruppin,³⁹ and, for rough silver films, Weitz *et al.*⁴⁰ The details and relative merits of the various theoretical models are discussed, *e.g.*, by Klar and Feldmann.³

A 1998 review by Barnes provides a comprehensive introduction to the interaction of metal surfaces with fluorophores, interpreting it in terms of tuning the photonic mode density (PMD).²¹ The presence of an interface (a metallic or dielectric surface) imposes boundary conditions, causing a reflection of the electromagnetic field. This changes the PMD in the vicinity of the surface, as a function of the phase difference between the incident and reflected fields at the fluorophore layer. If the fields are in-phase, the PMD is increased, and so are the emission rate and intensity. If the fields are out-of-phase, they are decreased. Thus, the emission lifetime should oscillate with metal-fluorophore separation, as the result of an interference effect. At short ranges, the fluorophore can couple to surface plasmon modes, which can

then radiate the energy, or decay to heat. This can enhance or quench the emission, respectively. According to one view of MEF, the fluorophore and plasmonic particle can form a single emitting complex, a *plasmophore*.^{1,41} At the closest separations, the emission is quenched due to coupling to lossy surface waves. If the dielectric spacer separating the metal and the fluorophore layer is thick enough (~ 100 nm and thicker), it can support waveguide modes, to which some radiation can couple. The fluorophore's emission frequency and linewidth (a function of the damping rate) are also expected to oscillate with spacer thickness, due to the changes in field intensity. The frequency shift and the change in damping rate are related to the in- and out-of-phase components of the reflected field, respectively. There have been very few measurements of frequency shifts in this context, and in some cases the experimental and predicted values differ by orders of magnitude.²¹

In 1975 Chance *et al.* studied the modification of the fluorescent lifetime of Eu^{3+} ions close to a metal film, finding oscillations in the lifetime as a function of ion-surface separation.⁴² In theoretical work published the same year, Chance *et al.* studied the effect of a partially reflective surface on the emission wavelength,⁴³ which the theory for fully reflective surface predicts will oscillate as a function of metal-fluorophore distance. They found that the frequency shift might actually be larger for a partially reflective mirror than for the perfect reflector case. Amos *et al.* studied the modification of the fluorescence lifetime of Eu^{3+} in the vicinity of thin metal mirrors,⁴⁴ finding a dependence on the metal film thickness, due to coupling to surface plasmon polaritons (SPP) on the far side of the metal film, an effect previously predicted from theory.³⁷ In later work, Amos *et al.* studied the interaction of fluorophores with corrugated metallic surfaces.⁴⁵ In 1984, Garoff *et al.* investigated the fluorescence spectra of Ru(II) trisbipyridine on silver island films on SiO_2 , compared to bare SiO_2 , and islands on Al. They found changes in the emission spectra between the different cases, but were unable to investigate the distance dependence.

In 1993, Kümmerlen *et al.* reported interaction at longer ranges, for the case of a silver nano-island film and the fluorescent dye Rhodamine 6G.⁴⁶ These authors reported two enhancement maxima – one at short range (5-10 nm), attributed to surface plasmon based amplification of the local field around the metallic nanoparticles; and a second peak at a larger separation (~ 60 nm), attributed to an increase in the fluorescence quantum yield, combined with resonant excitation due to a collective action of the nano-islands. Becker *et al.* reported similar long-range oscillations in fluorescence efficiency when varying the distance between an Al film and a fluorescent polymer layer; in addition, the authors reported shifts in the photoluminescence spectra, at different metal-fluorophore separations.⁴⁷

Following our previous investigations of the plasmon decay length of Au nano-island films,⁴⁸ we wished to explore a possible connection with the distance dependence in MEF. To this end, we assembled spacer layers on Au nano-island film samples, topped with the fluorescent complex ion ruthenium trisbipyridine, $[\text{Ru}(\text{bpy})_3]^{2+}$. This complex has a low quantum

yield of about 3%,⁴⁹ and so has potential for intensity enhancement through modification of the quantum yield. The complex features an MLCT (metal-to-ligand charge transfer) excited state, where the complex is better described as $\text{Ru}^{3+}(\text{bpy})_2(\text{bpy}^-)$. We used two types of samples, with average Au island in-plane diameters of ~ 20 nm and ~ 100 nm. Our group has extensively studied the morphology, fabrication process and plasmonic responses of these types of gold islands films.^{48,50-52} We used fluorophore-coated glass slides as controls, and studied the fluorescence intensity, peak wavelength and lifetime as a function of metal-fluorophore separation. To produce spacer coatings of controlled thickness, we utilized two methods. For thin coatings (2 – 72 nm) we used the polyelectrolyte (PE) layer-by-layer (LbL) method, developed by Decher,⁵³ in which alternate layers of oppositely-charged PEs are built in a stepwise fashion, *via* electrostatic interactions. This method is widely-used, is commonly noted for simplicity and reliability,^{54,55} and has been used in other MEF studies.^{6,56,57} For thicker coatings (up to 348 nm) we used SiO_x layers deposited by electron-beam assisted physical vapor deposition (EB-PVD).

2. Experimental section

2.1 Materials

The substrates used were microscope glass cover-slides (Schott AG borosilicate glass D263T No. 3, 22x22 mm², with $T_g \approx 557$ °C, supplied by Menzel-Gläser, Germany), cut to 22x9 mm². Gold (99.99%, Holland-Moran, Israel); SiO_2 pieces (99.99%, Kurt J. Lasker, USA); polyallylamine hydrochloride (PAH) (56 kDa, Sigma Aldrich); polystyrene sulfonate, sodium salt (PSS) (70 kDa, Polysciences Inc., Warrington, PA, USA); 3-aminopropyl trimethoxysilane (APTS) (Aldrich); Poly(ethyleneimine) (PEI) (Sigma, solution 50% w/v in H_2O); tris(bipyridine)ruthenium[II] oxalate; sodium chloride (Frutarom, Israel); methanol (absolute, Biolab, Israel); ethanol (anhydrous, Gadot or Biolab, Israel); H_2SO_4 (AR, 96%, Gadot); H_2O_2 (30%, Frutarom); and ammonium hydroxide (Frutarom), were used as received. Nitrogen was in-house supplied from liquid N_2 . All solutions were prepared using triply-distilled water.

2.2 Gold nano-island film fabricating

Glass slides were cleaned in freshly prepared “Piranha” solution ($\text{H}_2\text{O}_2:\text{H}_2\text{SO}_4$, 1:3 by volume) for 1 h, and washed three times with deionized water, then three times with triply distilled water, and finally with ethanol. (*Caution: “piranha” solution is extremely corrosive and boils upon mixing.*) 24 slides were placed on a plate, which was mounted in a cryo-HV evaporator (Key High Vacuum) equipped with a Maxtek TM-100 thickness monitor. The chamber was evacuated to a pressure of $2\text{-}3 \times 10^{-6}$ torr, and gold was evaporated onto the slides from a resistively-heated tungsten boat. The plate was rotated during evaporation to achieve homogenous deposition

on the slides. Gold was evaporated on the slides at a deposition rate of 0.01 nm/sec, to nominal thicknesses of 3 or 10 nm (the nominal thickness is the reading of the evaporator QCM thickness monitor, *i.e.*, the film mass thickness), forming films of 20 or 100 nm average in-plane diameter of the Au NPs. The slides were then annealed 10 h at 580 °C in a Ney Vulcan 3-550 furnace, at a 5 °C/min heating rate, then left to cool to room temperature inside the furnace.

2.3 Control sample fabrication

Glass slides were cut and cleaned with Piranha solution, as described above. The slides were then modified with an APTS solution (to form a positively charged surface for further adsorption) by overnight immersion in 1% APTS (by volume) in methanol, followed by thorough washing in methanol and drying, and coated with PSS, followed by 5 or 9 PAH/PSS bilayers (two samples each), using the LbL procedure described below.

2.4 Polyelectrolyte (PE) LbL assembly

The LbL procedure was carried out using the positive PE PAH and the negative PE PSS, 1.0 mM solutions (concentration calculated with respect to the monomer, corresponding to 0.093 mg mL⁻¹ PAH and 0.206 mg mL⁻¹ PSS) in 0.1 M NaCl in triply-distilled water. Au films prepared as detailed above were treated 10 min in a UV/Ozone apparatus (UVOCS Inc. model T10*10/OES/E), with the Au film facing the UV lamps. The samples were then washed 20 min in ethanol⁵⁸ and dried under a nitrogen stream. The slide to be coated was alternately immersed in vials containing the PE solutions for 15 min each, starting with PAH. After each adsorption step the slide was rinsed with water, dipped into an aqueous solution of 0.1 M NaCl, and immersed in the other PE solution. The thickness of each bilayer was determined in previous work, using spectroscopic ellipsometry, to be 2.09 ± 0.03 nm for 0.1 M NaCl, with a refractive index (RI) in the visible range of $n = 1.56$ and $k = 0$.⁴⁸ The adsorption and measurements were carried out in a climate-controlled laboratory, at a temperature of 22.5 ± 1.0 °C and a humidity of 50 ± 5 %. All adsorption steps were performed without stirring.

2.5 SiO_x coating

Continuous Au slides (produced according to a previously published procedure⁴⁸) and Au island slides prepared as detailed above were cleaned in a UV/Ozone apparatus, dipped in ethanol for 20 min and dried under a nitrogen stream. As silica has low adhesion to gold,⁵⁹ prior to deposition continuous Au slides were coated with APTS, by dipping the slide in a 0.1% v/v APTS solution in methanol for 15 minutes, followed by thorough washing in methanol and drying. Continuous Au and Au nano-island slides were then simultaneously coated with SiO_x (where $x \leq 2$, as oxygen was not added to the evaporation chamber) using electron-beam assisted physical vapor deposition, at a deposition rate of 0.15-0.2 nm/sec. The thickness was monitored *in-situ* using a quartz crystal microbalance, and accurately determined post deposition using

spectroscopic ellipsometry of coated continuous Au samples. This measurement also provided the RI of the coating in the visible range: $n = 1.46$, $k = 0$ (negligible absorption).

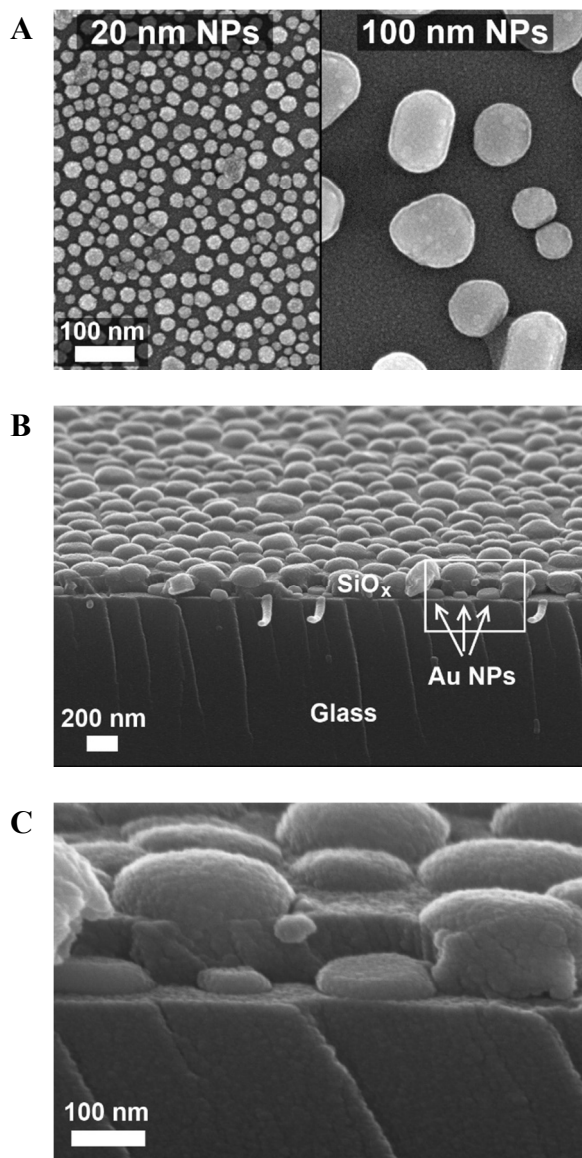


Fig. 1. Scanning electron microscopy (SEM) images of (A) pristine 20 nm and 100 nm Au NP samples (15 kV accelerating voltage); (B) fractured 100 nm NP sample coated with 100 nm SiO_x (10 kV accelerating voltage); (C) magnified view of the boxed area in B. Samples were coated with 2 nm (20 nm NPs) and 3 nm (100 nm NPs) of Cr for improved conductivity during imaging. Images were recorded using the in-lens SE detector. The elongated vertical features of the Au film and glass substrate are attributed to the breaking process.

2.6 Fluorophore deposition

Slides coated with PE films were terminated by the negatively charged PSS, to which the positively charged fluorescent complex $[\text{Ru}(\text{bpy})_3]^{2+}$ (0.03 M, 1.5 h) was adsorbed. To SiO_x coatings we first adsorbed PEI (1 mM monomer in H_2O , 15 min), followed by PSS and the fluorophore. The adsorption

period was chosen such that the extinction spectrum of control slides showed no further change. Following this step the back-side of the slides was gently scrubbed, to remove any adsorbed materials. The increase in extinction in control slides was used to calculate the surface coverage, which was found to be approximately 0.65 molecules / nm^2 .

2.7 Characterization

Extinction spectra at normal incidence were measured using a Varian Carey 50 Probe UV/Vis spectrophotometer. Measurement parameters: wavelength resolution, 1 nm; scan rate, 300 nm/min; average acquisition time per point, 0.2 sec. Air was used as the baseline.

SiO_x film thickness was measured in air using an Angstrom Advanced PhE-102 spectroscopic ellipsometer, at an angle of incidence of 70° , in the spectral range 300-800 nm, using 1 to 20 nm steps. Ellipsometric data were analyzed using Film Wizard software (Scientific Computing International, California, USA).

High-resolution scanning electron microscopy (HRSEM) images were obtained using a Carl Zeiss Ultra-55 Ultra-high-resolution SEM. Slides were coated with 2-3 nm of Cr prior to imaging to improve sample conductivity.

Steady-state fluorescence measurements were carried out using a HORIBA Jobin Yvon Fluorolog-3 spectrofluorometer, at 1 nm resolution, 0.2 sec averaging time, and 5 nm excitation and emission band-pass. The samples were placed on a solid sample holder, with the incident light at 454 nm hitting the sample at 30° from normal, and the light sensor at 60° off normal to the other side.

Fluorescence lifetime measurements were carried out using a custom-built instrument, comprising a Nd:YAG 355 nm third-harmonic laser as the excitation source, and a multi-channel scaling (MCS) detector. The system was continuously flushed with nitrogen gas during measurements, to prevent possible oxygen quenching.

3. Results and discussion

Fig. 1 shows scanning electron microscopy (SEM) images of some of the samples used in the present work. The fluorescence excitation/emission spectra of the fluorophore in solution are presented in Fig. 2A. The 100 nm Au NPs' extinction peaks exhibit a larger overlap with the fluorophore emission peak than those of the 20 nm NPs (Fig. 2A); both show only a small overlap with the excitation peak, meaning that photons scattered by the Au NPs are practically unable to excite the fluorophore layer. The $[\text{Ru}(\text{bpy})_3]^{2+}$ fluorophore was chosen by us in part based on its large Stokes shift, whereas many previous studies used small Stokes shift fluorophores (most organic dyes), precluding confident assignment of the observed effects to overlap with the emission or excitation peaks.

Fig. 3A shows an example of quenched and enhanced fluorescence of the fluorophore on 100 nm Au NPs. At small

NP-fluorophore separation the fluorescence is quenched due to non-radiative energy transfer between the excited state of the fluorophore and the plasmon modes of the NPs, while at the large separation a fluorescence enhancement is evident. The distance dependence of the fluorescence intensity for the two transducer types is presented in Fig. 3B. A maximal (ca. fivefold) enhancement is obtained for 100 nm Au NPs with a spacer thickness of about 60 nm, followed by a slow decrease, reaching the control level around 300 nm (the data point around 250 nm spacer thickness, showing an abnormally large enhancement, is assumed to be an outlier). The 20 nm Au NP samples exhibit mostly quenching, even at large separations. The distance-dependent intensity for both NP sizes is similar (see Fig. S1, Supporting Information). This type of behavior suggests a competition between two mechanisms – enhancement and quenching – where the former dominates the response for the 100 nm NPs, while the latter is dominant for

the 20 nm NPs, possibly as a result of the smaller spectral overlap with the fluorophore emission (Fig. 2A). The result is consistent with previous reports, noting the significance of a large spectral overlap between the plasmonic structures and the fluorophore emission peak.⁶⁰ A previous study of MEF concluded that maximal enhancement occurs when the LSPR peak is slightly higher in energy (40 – 120 meV) than the fluorophore emission peak, contrary to our present results.⁶¹ Another possible reason for the disparity between the two NP sizes is their different reflectivities – the peak reflectivity of 20 nm NPs is 10% (at 543 nm), compared to 27% (at 600 nm) for 100 nm NPs. At the very closest metal-fluorophore separation (~2 nm) charge-transfer could account for some of the observed quenching. As a tunnelling process, however, this pathway quickly becomes irrelevant for larger separations, and so will not be explored in depth here.

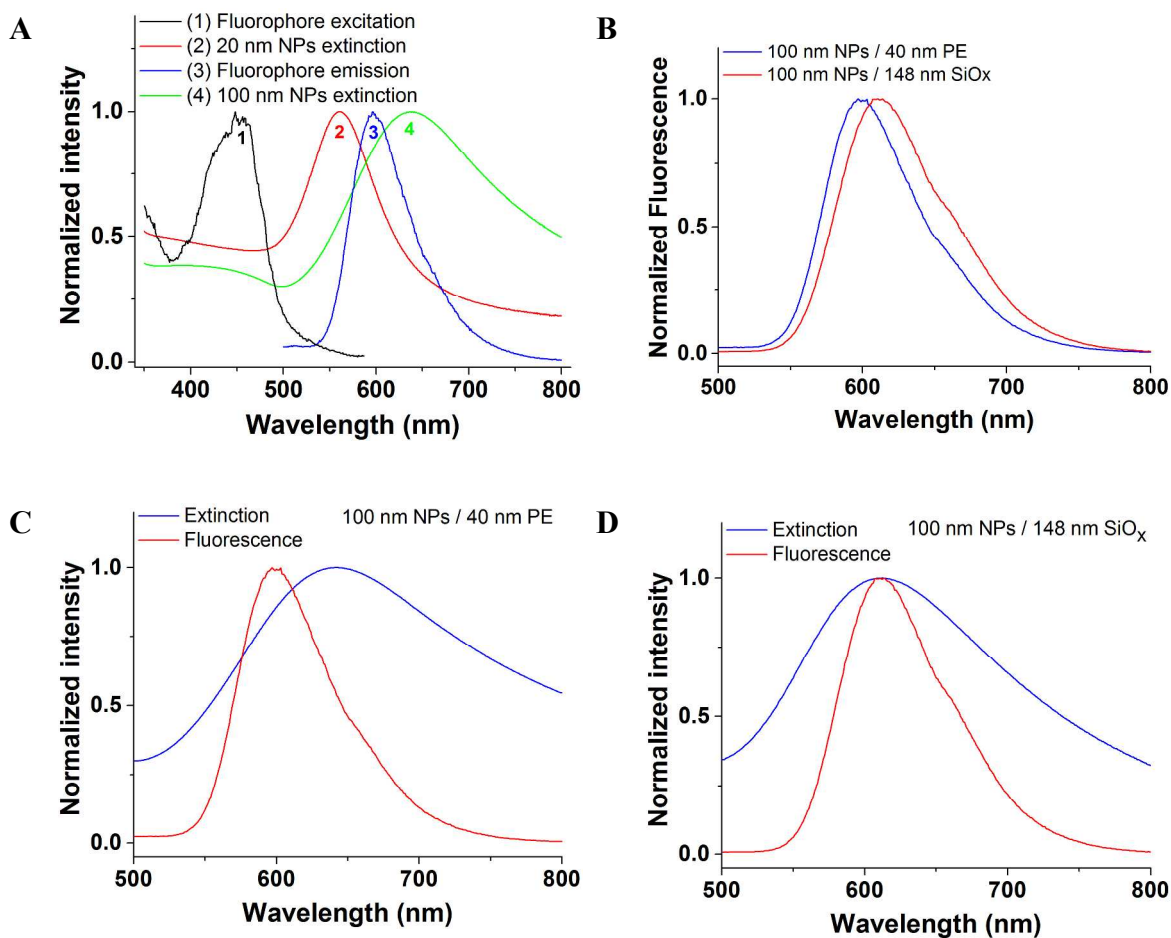


Fig. 2. (A) Normalized fluorescence emission and excitation for $[\text{Ru}(\text{bpy})_3]^{2+}$ on glass control slides, emission spectrum excited at 454 nm, excitation spectrum determined by measuring the emission at 605 nm, and scanning over different excitation wavelengths; and extinction spectra of 20 nm and 100 nm Au NP films, coated with 21 nm PE; (B) Normalized emission spectra for 100 nm NP samples, on two spacer thicknesses; (C, D) normalized emission and extinction spectra for two 100 nm NP samples, with a (C) 40 nm PE spacer and (D) 148 nm SiO_x spacer.

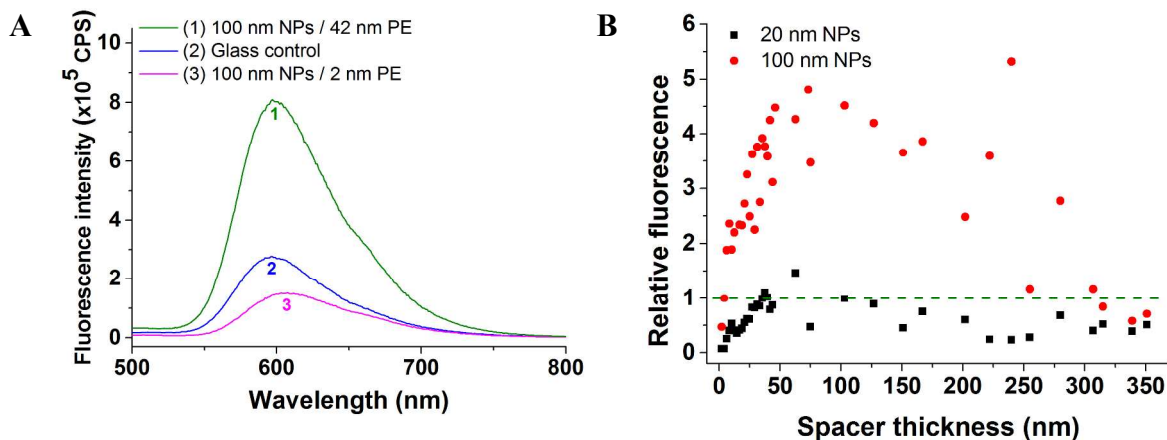


Fig. 3. (A) Emission spectra for a glass control sample and for 100 nm Au NP samples coated with $[\text{Ru}(\text{bpy})_3]^{2+}$ fluorophore on 2 nm and 42 nm PE spacers; (B) fluorescence intensity, relative to control samples without Au islands (dashed line), for 20 nm and 100 nm NP samples, coated with various thicknesses of PE (≤ 72 nm) or SiO_x (≥ 70 nm).

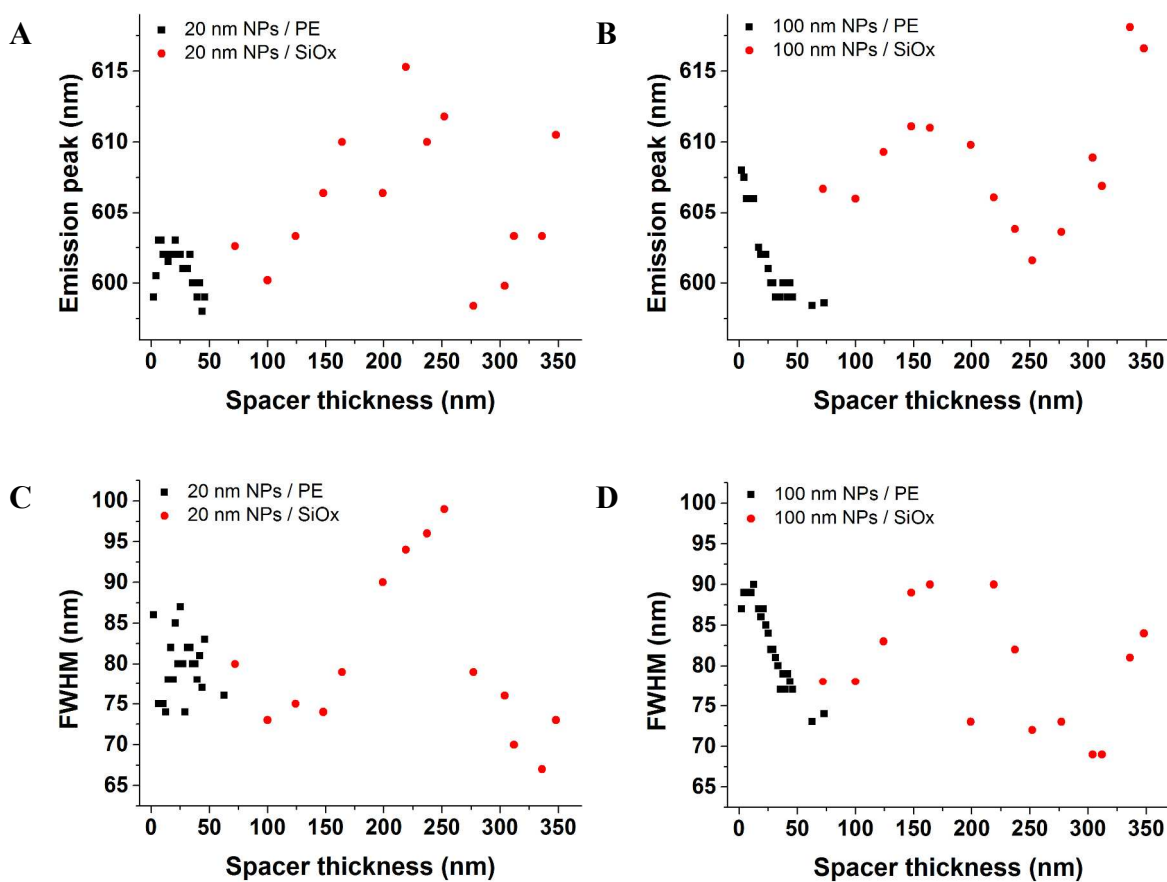


Fig. 4. Fluorescence emission peak wavelength (A, B) and linewidth, as full width at half maximum (FWHM) (C, D), for (A, C) 20 nm Au NP samples and (B, D) 100 nm NP samples, coated with various thicknesses of PE or SiO_x spacers (indicated).

The fluorophore emission peak shifts with spacer thickness. The fluorescence spectra for 100 nm NP samples at two spacer

thicknesses demonstrate a large shift in peak wavelength (Fig. 2B), and a similar behavior is observed for 20 nm NPs (Fig. S2,

Supporting Information). The plasmon peak extinction wavelength varies with spacer thickness, as previously shown by us.^{30,48} The variation of both the Au NP plasmon peak wavelength and the fluorophore emission peak wavelength leads to change of the spectral overlap as a function of spacer thickness; this is demonstrated for two 100 nm NP samples of different spacer thicknesses (Fig. 2 panels C, D). However, despite the difference in spectral overlap, the fluorescence intensity in both cases is similar (Fig. 3B; relative intensities are 3.58 and 3.65 for 40 and 148 nm spacers, respectively). This insensitivity to the spectral overlap seems to indicate that the fluorescence intensity difference between 20 and 100 nm NPs is related more to the aforementioned difference in reflectivity between the two, consistent with an enhancement mechanism based on reflected waves.

Fig. 4 shows the fluorescence emission peak wavelength and spectral width (as FWHM) as a function of spacer thickness. The variation for 100 nm NPs (Fig. 4 panels B, D) appears to be a sinusoidal oscillation, whereas the data for 20 nm NPs (Fig. 4 panels A, C) are not clear enough to permit such a conclusion. Emission peak shifts and linewidth changes have previously been predicted, as discussed above, but to our knowledge they are studied here for the first time as a function of fluorophore-plasmonic structure separation. The observed oscillation is consistent with the proposed explanation, relating the emission wavelength and linewidth to the field intensity variations resulting from interference of the incident and reflected waves.

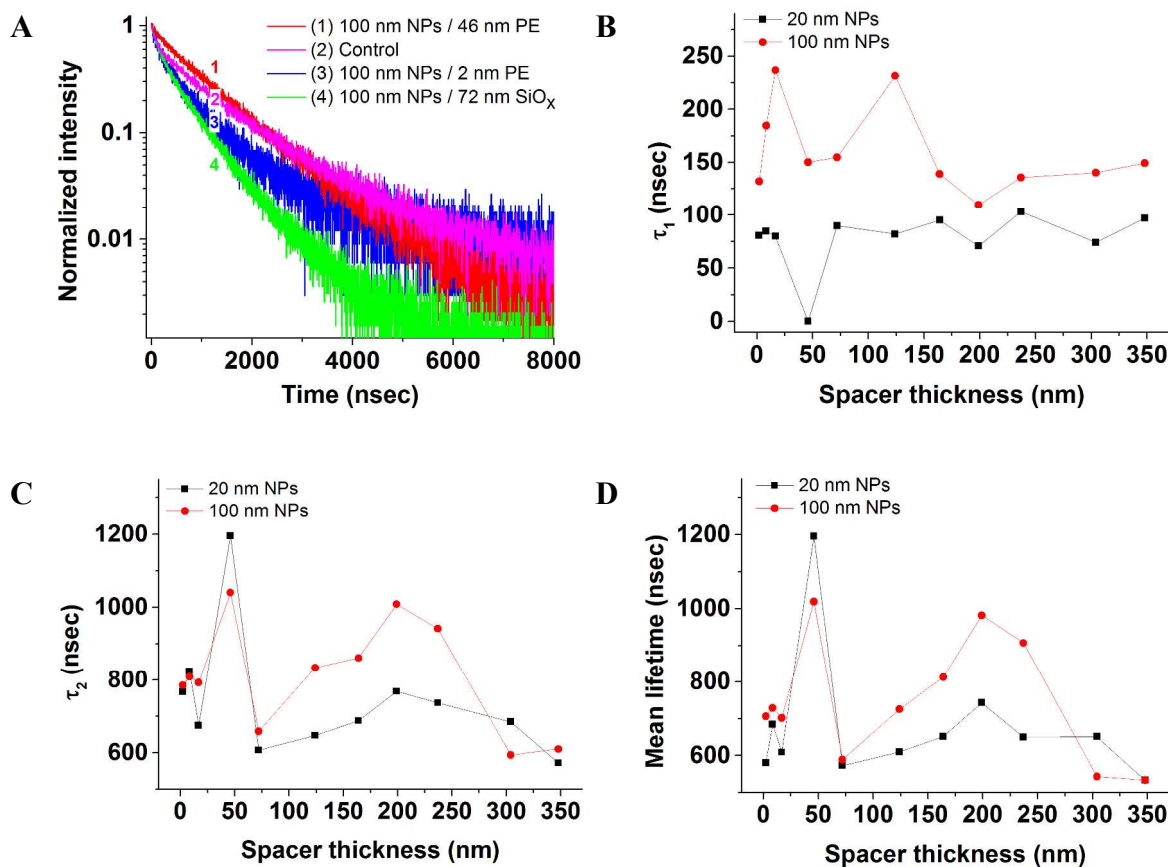


Fig. 5. (A) Fluorescence decay curves for a control slide and three 100 nm Au NP samples, coated with spacers of different thicknesses (indicated) and $[\text{Ru}(\text{bpy})_3]^{2+}$, excited at a wavelength of 355 nm; (B–D) the fast decay component lifetime τ_1 , slow decay component lifetime τ_2 , and mean fluorescence lifetime $\bar{\tau}$, respectively (see text) vs. spacer thickness.

The interaction of fluorophores with metallic surfaces or metallic NPs can result in three main effects, i.e., changes to the radiative rate, the non-radiative rate, and the excitation cross-section of the fluorophore.³ Steady-state fluorescence intensity measurements cannot distinguish between the possible causes of intensity changes; the latter can be elucidated using fluorescence lifetime measurement. Representative

fluorescence decay curves for fluorophore and spacer coated 100 nm NP films are shown in Fig. 5A.

The decay curves were fitted to a bi-exponential model:

$$I = I_0 + A_1 \exp\left(-\frac{t}{\tau_1}\right) + A_2 \exp\left(-\frac{t}{\tau_2}\right) \quad (6)$$

where I is the fluorescence intensity, I_0 is the baseline intensity, A_1 and A_2 are the amplitudes of the two exponentials, t is the time, and τ_1 and τ_2 are the fast and slow lifetimes, respectively.

Of the numerous definitions of mean or effective lifetimes, we utilize the definition used by Zhang *et al.*⁶²

$$\bar{\tau} = \frac{A_1\tau_1^2 + A_2\tau_2^2}{A_1\tau_1 + A_2\tau_2} \quad (7)$$

Fig. 5 panels B-D show the two lifetime components and the mean lifetime for the samples studied. Two glass control samples gave the following mean values: $\tau_1 = 118 \pm 5$ nsec, $\tau_2 = 1250 \pm 60$ nsec, $\bar{\tau} = 1190 \pm 60$ nsec. The decay process of the fluorophore on the Au nanoisland films is composed of a fast ($\tau_1 \sim 90$ -150 nsec) and a slow ($\tau_2 \sim 600$ -900 nsec) component. The fast component shows no clear trend; for the 20 nm NPs it is faster and for the 100 nm NPs it is slower than for the controls. The mean lifetime $\bar{\tau}$ is dominated by the slow component for both NP sizes. At the closest separation (2 nm spacer) a significantly shortened lifetime and strong intensity quenching are observed, indicating an accelerated non-radiative decay rate, as energy transfer to the NPs, and possibly charge-transfer between the NPs and fluorophore.

The plots indicate a long-range oscillation (Fig. 5D), with a peak lifetime around 50 nm ($\sim 1050 - 1200$ nsec) followed by a minimum and a second, lower maximum around 200 nm. Both τ_2 and $\bar{\tau}$ of the Au NP slides are shorter than those of the controls for essentially all the thicknesses. Literature reports generally show a correlation between fluorescence enhancement and shortened lifetimes, as increased fluorescence rates make the radiative process more competitive with non-radiative decay paths. Interestingly, this is not the case here (see correlation plots in Fig. S3, Supporting Information). For instance, the lifetime for 20 nm NP samples is shorter than that of the controls for all thicknesses, despite displaying fluorescence quenching relative to the controls. The distance-dependent profile for the lifetime in both cases seems to have only a weak correlation with the fluorescence intensity profile – for example, though spacer thicknesses of ~ 46 -72 nm display similar enhancement factors of 4-5 (Fig. 3), their lifetimes are vastly different.

The shape of the mean lifetime plot (Fig. 5D) is remarkably similar to that of the Eu^{3+} / mirror system, studied by Drexhage *et al.*^{36,63} and later analyzed by Chance *et al.*^{37,42} This provides further support to the view that the collective behavior of the NP film is akin in some ways to a continuous metal mirror.³⁰

While most studies in the field of MEF present a distance dependence up to 20-30 nm, effects beyond this range were reported by several groups, as discussed in the Introduction. While the samples used in the present work are composed of random Au nano-island arrays, and not smooth continuous films, these nano-islands can act as a mirror by far-field interaction.^{30,64} As mentioned earlier, metal mirrors were reported to cause large oscillations in the fluorescent lifetime of nearby fluorophores, as a function of metal-fluorophore separation.^{42,44} The lifetime plots in those studies exhibited an initial maximum at quite short separations (~ 20 nm), followed by a decrease, with a second peak around 200 nm. These values match our results quite nicely, despite the fact that a NP array introduces a phase shift in the reflected field which is different

from that introduced by a continuous metal film, as we have previously shown.³⁰

Our results show a strong oscillation of the emission peak wavelength and peak width (FWHM) as a function of metal-fluorophore separation (Fig. 4). Interestingly, the magnitude of the measured shifts is much larger than that discussed by Barnes, who mentioned shifts in the MHz to GHz range,²¹ while our measured shifts are in the THz range (a wavelength shift from 605 to 610 nm is about 4 THz in the frequency domain). The magnitude of the emission peak shift is similar to that reported by Holland *et al.* for shifts in the plasmon resonance of metal NPs above a metallic surface.⁶⁵

4. Conclusions

Long-range four-fold fluorescence enhancement (for 100 nm Au NPs) and THz-scale oscillatory shifts of the emission wavelength and linewidth are observed for a fluorophore layer separated from a plasmonic gold nano-island film by a dielectric spacer. While such an oscillation is predicted by theory, to our knowledge this is the first detailed study of the distance dependence of the emission peak and linewidth of a fluorophore above a metal surface; it is our hope that these results will assist the development of better models for such systems. The fluorophore used here, $\text{Ru}(\text{bpy})_3^{2+}$, has an intrinsically low quantum yield and a large Stokes shift, enabling sensitive detection of the relevant interactions.

In the present work, fluorescence lifetime measurements revealed a shortened fluorescence lifetime for almost all studied samples, compared to controls (glass slides without Au islands). However, there seems to be no correlation between fluorescence intensity and lifetime; the lifetimes for 20 nm and 100 nm Au NP samples are similar, despite the substantial difference in intensity. The relationship between fluorescence lifetime and intensity is not trivial, involving several mechanisms, such as interference between incoming and reflected excitation, quenching, and possible plasmon-fluorophore coupled emission (plasmophore). The changing relative contributions of each process combine to form the complex observed relationship.

Our original motivation for conducting this work was to examine a possible connection between the MEF distance dependence profile and the plasmon decay length (decay of the evanescent field from the Au NPs), which we have previously measured for these films.⁴⁸ The present results indicate no such connection. The measured decay lengths for the 20 and 100 nm NPs are approximately 3 nm and 20 nm, and yet they present the same distance dependence for intensity (though with different intensities), lifetime and spectral properties (maximum wavelength, linewidth). It appears that, at least for these relatively dense films, the collective behavior of the reflective NP films dominates any short-range decay length differences. Future work may use a similar system of fluorophore and spacers to reveal the ratio between plasmon decay length and NP separation for which the long-range and oscillatory behavior emerges, marking the collective behavior of Au NPs.

Acknowledgements

The authors express their deep gratitude to Dr. Gerhard Wagenblast, T. Altenbeck and Th. Ohmer (BASF SE, Ludwigshafen, Germany) for assisting with the fluorescence lifetime measurements. Support of this work by the Israel Science Foundation, grant No. 1251/11, and by the Gerhardt M. J. Schmidt Minerva Center of Supramolecular Architectures, is gratefully acknowledged. I. R. is Incumbent of the Agnes Spencer Professorial Chair of Physical Chemistry. The electron microscopy studies were conducted at the Irving and Cherna Moskowitz Center for Nano and Bio-Nano Imaging, Weizmann Institute of Science. This research is made possible in part by the historic generosity of the Harold Perlman family.

Notes and references

^a Dept. of Materials and Interfaces, Weizmann Institute of Science, Rehovot 7610001, Israel; present address for O.K. - Dept. of Chemistry, Northwestern University, Evanston, IL 60208-3113, USA; E-mail: kedem.ofer@northwestern.edu

^b BASF SE, Advanced Materials Research, Dept. of Material Physics, 67056 Ludwigshafen, Germany.

Electronic Supplementary Information (ESI) available: Detailed relative fluorescence intensities of 20 nm Au NP samples; emission spectra of the fluorophore on two different spacer thicknesses on 20 nm Au NP samples; correlation plots of lifetime and relative fluorescence intensities. See DOI: 10.1039/b000000x/

- J. R. Lakowicz, K. Ray, M. Chowdhury, H. Szmecinski, Y. Fu, J. Zhang and K. Nowaczyk, *The Analyst*, 2008, **133**, 1308-1346.
- W. Deng and E. M. Goldys, *Langmuir*, 2012, **28**, 10152-10163.
- T. A. Klar and J. Feldmann, in *Complex-shaped Metal Nanoparticles: Bottom-Up Syntheses and Applications*, eds. T. K. Sau and A. L. Rogach, Wiley-VCH, Weinheim, 1st edn., 2012, pp. 395-427.
- T. Ming, H. Chen, R. Jiang, Q. Li and J. Wang, *J. Phys. Chem. Lett.*, 2012, **3**, 191-202.
- Y.-H. Chan, J. Chen, S. E. Wark, S. L. Skiles, D. H. Son and J. D. Batteas, *ACS Nano*, 2009, **3**, 1735-1744.
- K. Ray, R. Badugu and J. R. Lakowicz, *Chem. Mater.*, 2007, **19**, 5902-5909.
- X. Gu, Y. Wu, L. Zhang, Y. Liu, Y. Li, Y. Yan and D. Wu, *Nanoscale*, 2014, **6**, 8681-8693.
- H. Tanaka, M. Mitsuishi and T. Miyashita, *Chem. Lett.*, 2005, **34**, 1246-1247.
- P. P. Pompa, L. Martiradonna, A. D. Torre, F. D. Sala, L. Manna, M. De Vittorio, F. Calabi, R. Cingolani and R. Rinaldi, *Nat. Nanotechnol.*, 2006, **1**, 126-130.
- O. Stranik, R. I. Nooney, C. McDonagh and B. D. MacCraith, *Plasmonics*, 2007, **2**, 15-22.
- Y. Zhang, A. Dragan and C. D. Geddes, *J. Phys. Chem. C*, 2009, **113**, 12095-12100.
- M. P. Singh and G. F. Strouse, *J. Am. Chem. Soc.*, 2010, **132**, 9383-9391.
- H. Aouani, J. r. m. Wenger, D. Gérard, H. Rigneault, E. s. Devaux, T. W. Ebbesen, F. Mahdavi, T. Xu and S. Blair, *ACS Nano*, 2009, **3**, 2043-2048.
- J. R. Lakowicz, J. Malicka, S. D'Auria and I. Gryczynski, *Anal. Biochem.*, 2003, **320**, 13-20.
- M. L. Viger, L. S. Live, O. D. Therrien and D. Boudreau, *Plasmonics*, 2008, **3**, 33-40.
- J. Zhang, Y. Fu and J. R. Lakowicz, *J. Phys. Chem. C*, 2007, **111**, 1955-1961.
- L. Zhao, T. Ming, H. Chen, Y. Liang and J. Wang, *Nanoscale*, 2011, **3**, 3849-3859.
- K. Ray, M. H. Chowdhury, J. Zhang, Y. Fu, H. Szmecinski, K. Nowaczyk and J. R. Lakowicz, in *Optical Sensor Systems in Biotechnology*, ed. G. Rao, 2010, pp. 29-72.
- G. R. Bourret, T. Ozel, M. Blaber, C. M. Shade, G. C. Schatz and C. a. Mirkin, *Nano Lett.*, 2013, **13**, 2270-2275.
- P. Anger, P. Bharadwaj and L. Novotny, *Phys. Rev. Lett.*, 2006, **96**, 3-6.
- W. L. Barnes, *J. Mod. Opt.*, 1998, **45**, 661-699.
- E. Fermi, *Rev. Mod. Phys.*, 1932, **4**, 87-132.
- B. I. Ipe, K. G. Thomas, S. Barazzouk, S. Hotchandani and P. V. Kamat, *J. Phys. Chem. B*, 2002, **106**, 18-21.
- C. Fan, S. Wang, J. W. Hong, G. C. Bazan, K. W. Plaxco and A. J. Heeger, *Proc. Natl. Acad. Sci. U. S. A.*, 2003, **100**, 6297-6301.
- N. Akbay, J. R. Lakowicz and K. Ray, *J. Phys. Chem. C*, 2012, **116**, 10766-10773.
- J. Malicka, I. Gryczynski, Z. Gryczynski and J. R. Lakowicz, *Anal. Biochem.*, 2003, **315**, 57-66.
- R. I. Nooney, O. Stranik, C. McDonagh and B. D. MacCraith, *Langmuir*, 2008, **24**, 11261-11267.
- A. Wokaun, H.-P. Lutz, A. P. King, U. P. Wild and R. R. Ernst, *J. Chem. Phys.*, 1983, **79**, 509-514.
- Y. Teng, K. Ueno, X. Shi, D. Aoyo, J. Qiu and H. Misawa, *Ann. Phys. (Berlin)*, 2012, **524**, 733-740.
- O. Kedem, T. Sannomiya, A. Vaskevich and I. Rubinstein, *J. Phys. Chem. C*, 2012, **116**, 26865-26873.
- V. V. Klimov, M. Duclouy and V. S. Letokhov, *Quantum Electron.*, 2001, **31**, 569-586.
- J. R. Lakowicz, *Anal. Biochem.*, 2001, **298**, 1-24.
- J. R. Lakowicz, J. Malicka, I. Gryczynski, Z. Gryczynski and C. D. Geddes, *J. Phys. D: Appl. Phys.*, 2003, **36**, R240-R249.
- J. R. Lakowicz, *Anal. Biochem.*, 2005, **337**, 171-194.
- E. Fort and S. Grésillon, *J. Phys. D: Appl. Phys.*, 2008, **41**, 013001.
- K. H. Drexhage, in *Progress in Optics XII*, ed. E. Wolf, Elsevier, 1974, pp. 163-232.
- R. R. Chance, A. Prock and R. Silbey, in *Adv. Chem. Phys.*, eds. I. Prigogine and S. A. Rice, John Wiley & Sons, 1978, vol. 37, pp. 1-65.
- J. Gersten and A. Nitzan, *J. Chem. Phys.*, 1981, **75**, 1139-1139.
- R. Ruppin, *J. Chem. Phys.*, 1982, **76**, 1681-1681.
- D. A. Weitz, S. Garoff, J. I. Gersten and A. Nitzan, *J. Chem. Phys.*, 1983, **78**, 5324-5338.
- T. Ming, L. Zhao, H. Chen, K. C. Woo, J. Wang and H.-q. Lin, *Nano Lett.*, 2011, **11**, 2296-2303.
- R. R. Chance, A. H. Miller, A. Prock and R. Silbey, *J. Chem. Phys.*, 1975, **63**, 1589-1595.
- R. Chance, A. Prock and R. Silbey, *Phys. Rev. A*, 1975, **12**, 1448-1452.
- R. M. Amos and W. L. Barnes, *Phys. Rev. B*, 1997, **55**, 7249-7254.
- R. Amos and W. Barnes, *Phys. Rev. B*, 1999, **59**, 7708-7714.
- J. Kümmerlen, A. Leitner, H. Brunner, F. R. Aussenegg and A. Wokaun, *Mol. Phys.*, 1993, **80**, 1031-1046.
- H. Becker, S. Burns and R. Friend, *Phys. Rev. B*, 1997, **56**, 1893-1905.
- O. Kedem, A. B. Tesler, A. Vaskevich and I. Rubinstein, *ACS Nano*, 2011, **5**, 748-760.
- M. J. Cook, A. P. Lewis, G. S. G. McAuliffe, V. Skarda, A. J. Thomson, J. L. Glasper and D. J. Robbins, *J. Chem. Soc. Perk. T. 2*, 1984, 1293-1301.
- T. Karakouz, D. Holder, M. Goomanovsky, A. Vaskevich and I. Rubinstein, *Chem. Mater.*, 2009, **21**, 5875-5885.

51. T. Karakouz, A. B. Tesler, T. A. Bendikov, A. Vaskevich and I. Rubinstein, *Adv. Mater.*, 2008, **20**, 3893-3899.
52. A. B. Tesler, L. Chuntonov, T. Karakouz, T. A. Bendikov, G. Haran, A. Vaskevich and I. Rubinstein, *J. Phys. Chem. C*, 2011, **115**, 24642-24652.
53. G. Decher, J. Hong and J. Schmitt, *Thin Solid Films*, 1992, **210-211**, 831-835.
54. R. von Klitzing, J. E. Wong, W. Jargerc and R. Steitz, *Curr. Opin. Colloid In.*, 2004, **9**, 158-162.
55. G. Decher, *Science*, 1997, **277**, 1232-1237.
56. N. Gandra, C. Portz, L. Tian, R. Tang, B. Xu, S. Achilefu and S. Singamaneni, *Angew. Chem., Int. Ed. Engl.*, 2014, **53**, 866-870.
57. G. Schneider, G. Decher, N. Nerambourg, R. Praho, M. H. V. Werts and M. Blanchard-Desce, *Nano Lett.*, 2006, **6**, 530-536.
58. H. Ron, S. Matlis and I. Rubinstein, *Langmuir*, 1998, **14**, 1116-1121.
59. L. He, E. A. Smith, M. J. Natan and C. D. Keating, *J. Phys. Chem. B*, 2004, **108**, 10973-10980.
60. N. I. Cade, T. Ritman-Meer, K. Kwaka and D. Richards, *Nanotechnology*, 2009, **20**, 285201.
61. Y. Chen, K. Munechika and D. S. Ginger, *Nano Lett.*, 2007, **7**, 690-696.
62. Y. Zhang, K. Aslan, M. J. R. Previte, S. N. Malyn and C. D. Geddes, *J. Phys. Chem. B*, 2006, **110**, 25108-25114.
63. K. H. Drexhage, *J. Lumin.*, 1970, **1-2**, 693-701.
64. T. Sannomiya, T. E. Balmer, C. Hafner, M. Heuberger and J. Vörös, *Rev. Sci. Instrum.*, 2010, **81**, 053102.
65. W. R. Holland and D. G. Hall, *Phys. Rev. Lett.*, 1984, **52**, 1041-1044.